Modeling Earth Systems and Environment
https://doi.org/10.1007/s40808-023-01858-4

ORIGINAL ARTICLE

An evaluation of WRF urban canopy models over Bengaluru, India

Heather S. Sussman[1,2] · Aiguo Dai[2] · Ajay Raghavendra[3] · Liming Zhou[2]

Received: 19 April 2023 / Accepted: 4 September 2023

Abstract
Numerical modeling of urban climate is essential for understanding mechanisms of the urban heat island (UHI) phenomenon. However, models must first be evaluated to identify their limitations. Over India, the evaluation of the Weather Research and Forecasting (WRF) model is limited. Here, WRF was evaluated over Bengaluru, India diurnally during the dry and wet seasons. Simulations were performed for cases using no urban canopy model (No-UCM), the single-layer UCM (SLUCM), and the multi-layer UCM (MLUCM) with the Mellor-Yamada-Janjić and the Bougeault and Lacarrerè planetary boundary layer (PBL) schemes. The simulations were compared to land surface temperature (LST) observations from the Moderate Resolution Imaging Spectroradiometer for their biases in urban LST, non-urban LST, and UHI intensity. Absorbed shortwave radiation, net longwave radiation, sensible heat, and latent heat were investigated for their possible role in driving the LST biases since they are calculated differently depending on which UCM is used. Results show urban LST was more sensitive to UCM choice than PBL scheme and the use of an UCM reduced urban LST biases, leading to improved simulations of the UHI. Non-urban LST was insensitive to UCM and PBL choice. For the best case, urban LST was underestimated by less than 1 °C during the dry season day and night, and was overestimated by 1.88 °C and 0.08 °C in the wet season day and night. In general, the SLUCM had the least bias for urban LST and UHI intensity due to a near-zero latent heat flux in No-UCM, too much trapping of shortwave and longwave radiation by the MLUCM during daytime, and too much surface cooling at nighttime by the MLUCM. These results can inform future WRF studies that evaluate UHI mitigation strategies over Bengaluru on the best model physics to use.

Keywords Bengaluru · India · Planetary boundary layer (PBL) · Urban canopy model (UCM) · Urban heat island (UHI) · Weather Research and Forecasting (WRF)

Introduction

Urbanization impacts

More than half of the world's population lives in urban areas, which continues to increase (Grimm et al. 2008). While increased urbanization fosters commerce and leisure opportunities, urbanization can potentially harm the environment and those who live in and visit cities. For example, increased emissions due to manufacturing and vehicular traffic can degrade air quality (Ramachandran et al. 2012), which can increase the risk of respiratory illnesses (Filho et al. 2018). Additionally, urban sprawl and less natural vegetation can impact the ability of residents to enjoy nature and possibly impact well-being (Andersson 2006; van den Berg et al. 2015). Urbanization can also affect regional climate and local economy. For example, Kishtawal et al. (2010) showed an increase in the frequency of heavy precipitation episodes over Indian cities during the monsoon season due to urbanization, and such changes in monsoon rainfall could affect crop yield in India (Parthasarathy 1984).

One urbanization impact often studied is the urban heat island (UHI) phenomenon, which refers to the tendency of urban areas to be warmer than their non-urban surroundings (Oke 1982). The UHI phenomenon is of particular concern,

✉ Heather S. Sussman
Heather.S.Sussman@usace.army.mil

1 U.S. Army Engineer Research and Development Center–Geospatial Research Laboratory, 7701 Telegraph Rd., Alexandria, VA 22315, USA

2 Department of Atmospheric and Environmental Sciences, University at Albany, State University of New York, 1400 Washington Ave., Albany, NY 12222, USA

3 AASF#3 New York Army National Guard, 330 Old Niskayuna Rd., Latham, NY 12110, USA

Published online: 29 September 2023

especially in a warming climate, due to an increased risk of heat exhaustion and higher energy demands for cooling (Filho et al. 2018). The UHI effect arises due to urban surface properties. For example, decreased urban vegetation can reduce evapotranspiration and associated cooling, which leads to higher Bowen ratios. Consequentially, urban surfaces can warm faster and store more heat than non-urban surfaces during daytime, and retain that heat through a slow release at nighttime (Taha 1997). Decreased vegetation and more buildings can also increase surface roughness, which can decrease near-surface wind speed and result in less cooling via surface heat fluxes and thermal advection (Garratt 1994; Zhou et al. 2004).

Urbanization modeling

The UHI phenomenon has been studied using weather station observations, satellite data, and numerical modeling across the globe (e.g., Zhou et al. 2004; Hung et al. 2005; Imran et al. 2018). Numerical modeling can be advantageous since it can help scientists better understand UHI mechanisms and enable urban planners to test mitigation strategies. In order to develop optimal mitigation strategies, an in-depth understanding of the urban environment within a particular city is required (Lenhölzer and Van der Wulp 2010). However, prior to testing any mitigation strategies using numerical simulations, models need to be evaluated against observations to identify their biases and limitations.

The Weather Research and Forecasting (WRF) model is often coupled to an urban canopy model (UCM) to study the urban environment (Chen et al. 2011). UCMs simulate the exchange of energy and momentum between the urban surface and the atmosphere (Morini et al. 2018). Three UCM options exist in WRF in addition to the default setup without an UCM (No-UCM). With No-UCM, urban surfaces are represented by a roughness length of 0.8 m, a fixed surface albedo of 0.15, a volumetric heat capacity of 3.0 MJ m^{-3} K^{-1}, and a thermal conductivity of 3.24 W m^{-1} K^{-1} to represent heat storage in urban buildings and roads (Liu et al. 2006). The single-layer UCM (SLUCM), which was developed by Kusaka et al. (2001) and Kusaka and Kimura (2004), represents urban geometry by infinitely long street canyons. In the SLUCM, shortwave and longwave radiation in the street canyons can be shadowed, reflected, and trapped, and an exponential wind profile is prescribed to determine the wind speed in the canyon from the wind speed above the canyon (i.e., at the lowest model layer). The building effect parameterization (BEP) is a multi-layer UCM (MLUCM) developed by Martilli et al. (2002) that considers the three-dimensional nature of urban surfaces and the vertical distribution of sources and sinks of heat and momentum through the whole urban canopy and planetary boundary layer (PBL). The MLUCM scheme also includes the effects of vertical walls, horizontal streets, and roofs on momentum, turbulent kinetic energy, and potential temperature. As in the SLUCM, the shadowing, reflection, and trapping of both shortwave and longwave radiation also occurs in the MLUCM. The final UCM option was developed by Salamanca and Martilli (2010) and is an extension of the BEP/MLUCM scheme through the coupling to a building energy model (BEM). The BEM considers the diffusion of heat through walls, roofs, and floors, radiation exchanged through windows, longwave radiation exchanged between indoor surfaces, and generation of heat due to occupants and equipment. Overall, the evaluation of UCMs is an ongoing area of research with differing and region-dependent conclusions (e.g., Salamanca et al. 2011; Jandaghian and Beradi 2020).

While there have been numerous urban modeling studies over North America, Europe, and East Asia (e.g., Hung et al. 2005; Salamanca et al. 2011; Segura et al. 2021); Veena et al. (2020) remarked that such studies are limited over India compared to the number of observational studies investigating urbanization impacts. Most prior modeling studies over India have analyzed the impact of increased urbanization on monsoon rainfall (Shastri et al. 2015; Paul et al. 2018). A secondary theme in previous urban modeling studies over India is the impact of land cover change by either using WRF to demonstrate how increased urbanization has caused UHIs (Sati and Mohan 2018; Mohan et al. 2020; Kedia et al. 2021) or the sensitivity of WRF-simulated UHIs to different land cover datasets (Bhati and Mohan 2018; Patel et al. 2020). Of these previous studies over India, only Paul et al. (2018) evaluated WRF's sensitivity to UCM choice by comparing cases using No-UCM, the SLUCM, and the MLUCM. They found that the MLUCM performed best in simulating eight extreme rainfall cases during summer over Mumbai. However, Paul et al. (2018) noted that to achieve robust results, more cases should be simulated and in different seasons. Additionally, Mumbai is located on the northwest coast of India at an elevation of 0.3 m. Therefore, the findings for Mumbai may not be valid for other Indian cities given that cities have different geographic features, climate, and urban surface characteristics. Additionally, different forcing data can be used to run WRF, which may contribute to different model performance. Paul et al. (2018) used ERA-Interim reanalysis of $0.75° \times 0.75°$ resolution as forcing data. The newly available ERA5 reanalysis, which has higher spatial and temporal resolution, needs to be evaluated.

Paul et al. (2018) also tested the sensitivity of their WRF simulations to the PBL scheme, specifically the Mellor-Yamada-Janjić (MYJ; Janjić 2002) and the Bougeault and Lacarrerè (BouLac; Bougeault and Lacarrerè 1989) schemes, and found BouLac to perform better. These schemes were chosen since the MLUCM can only be used with MYJ or BouLac (Ferrero et al. 2018).

Both MYJ and BouLac are one-and-a-half order prognostic turbulent kinetic energy (TKE) schemes with local closure (Xie et al. 2012). Therefore, the turbulent fluxes are computed at each grid point using the mean values of atmospheric variables and/or their gradients at the given point. In the governing equations of these PBL schemes, the momentum, heat, and TKE coefficients are identical in BouLac, whereas they differ from each other in MYJ (Xie et al. 2012). Additionally, the BouLac scheme has a non-local counter gradient term for convective conditions (Xie et al. 2012). While the MYJ scheme is more commonly used (Banks et al. 2015), the BouLac scheme was designed for use with the MLUCM (Martilli et al. 2002). Therefore, both should be evaluated when using the MLUCM since the PBL plays an important role in urban climate (Garratt 1994).

Due to limited studies on the evaluation of WRF with different UCMs and PBL schemes in India, more research is needed to evaluate WRF's ability to simulate UHIs. One particular city that is markedly different from Mumbai is Bengaluru, which is centrally located in southern India (city center: 12.97°N, 77.59°E) on the Deccan Plateau at an elevation of 900 m. Bengaluru is the third most populous city in India with a current population of ~ 13 million and was once known as the *"Garden City"* of India, but is now known as the *"Silicon City"* due to the increased presence of the information technology industry (Sudhira et al. 2007). To our knowledge, only Ajilesh et al. (2019), Sahoo et al. (2020), and Rakesh et al. (2021) have used WRF over Bengaluru. These studies focused on WRF's skill in simulating extreme rainfall. Ajilesh et al. (2019) did not couple WRF to an UCM, Sahoo et al. (2020) coupled WRF to the SLUCM, and Rakesh et al. (2021) coupled WRF to the MLUCM. None of the studies evaluated their respective simulations with different UCMs. Therefore, it is unclear how WRF performs when coupled with different UCM and PBL schemes in simulating Bengaluru's UHI.

The goal of this study is to perform an evaluation of WRF to determine which UCM (No-UCM, SLUCM, or MLUCM) and PBL scheme (MYJ or BouLac) performs best in capturing the observed UHI over Bengaluru. The BEP + BEM UCM will not be evaluated due to its high computation time, thus making it rarely used (Kwok and Ng 2021). WRF simulations were evaluated during the dry (December-January–February; DJF) and wet (August–September–October; ASO) seasons during daytime and nighttime. This seasonal comparison was chosen to be consistent with recent empirical analyses on the characteristics and controls of the UHI in Bengaluru (Sussman et al. 2019, 2021). Results will enable future studies to use the best performing UCM and PBL scheme combination to investigate mechanisms and test mitigation strategies of Bengaluru's UHI.

Data and methods

WRF simulations

WRF v4.2.2 (Skamarock et al. 2019) was used to simulate surface skin temperature (TSK) in Bengaluru and its nearby non-urban surroundings. TSK is the surface radiative temperature that WRF calculates from the surface energy balance. A schematic of the 12 simulations performed that vary by model physics and season is shown in Fig. 1. All simulations began at 00 UTC on the first day listed for DJF and ASO in Fig. 1 and ran through the last day listed. The first 24 h of all simulations was used as the spin-up period, which left 60 days for analysis. A 60-day simulation was analyzed so that variability within a season could be captured and to have enough daily samples to produce robust results without the increased computation time of simulating a full season. These simulations were performed for 2018 since it is most representative of current conditions and to be consistent with Sussman et al. (2019, 2021) who analyzed Bengaluru's UHI for 2003–2018.

All simulations were performed over a single domain of 150 km × 150 km with 1 km grid spacing focused on Bengaluru's city center (Fig. 2). Each simulation used Moderate Resolution Imaging Spectroradiometer (MODIS) Aqua and Terra combined annual-mean land cover from Collection 6 (MCD12Q2) for 2018 at 1 km resolution (Fig. 2). The use of annual-mean land cover should not impact seasonal simulations since Sussman et al. (2019) showed that urban land cover in Bengaluru increased at a rate of approximately 1% per year from 2003 to 2018. Therefore, the intra-annual changes in urban land cover are small. The MODIS land cover dataset defines land cover type according to the classifications developed by the International Geosphere-Biosphere Programme (IGBP). The IGBP defines urban and

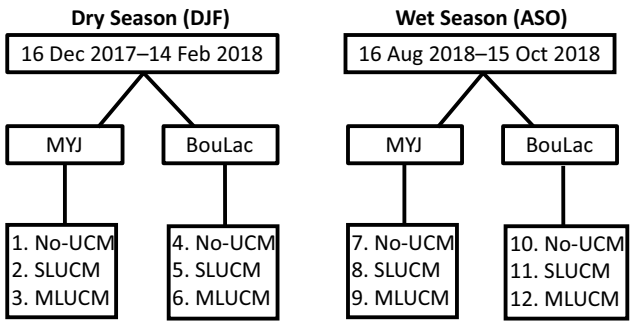

Fig. 1 Schematic summarizing the 12 simulations performed in this study that vary by season, i.e., December-January–February (DJF) and August–September-October (ASO), planetary boundary layer scheme, i.e., Mellor-Yamada-Janjić (MYJ) and Bougeault and Lacarrerè (BouLac) and urban canopy model (UCM), i.e., No-UCM, single-layer UCM (SLUCM), and multi-layer UCM (MLUCM)

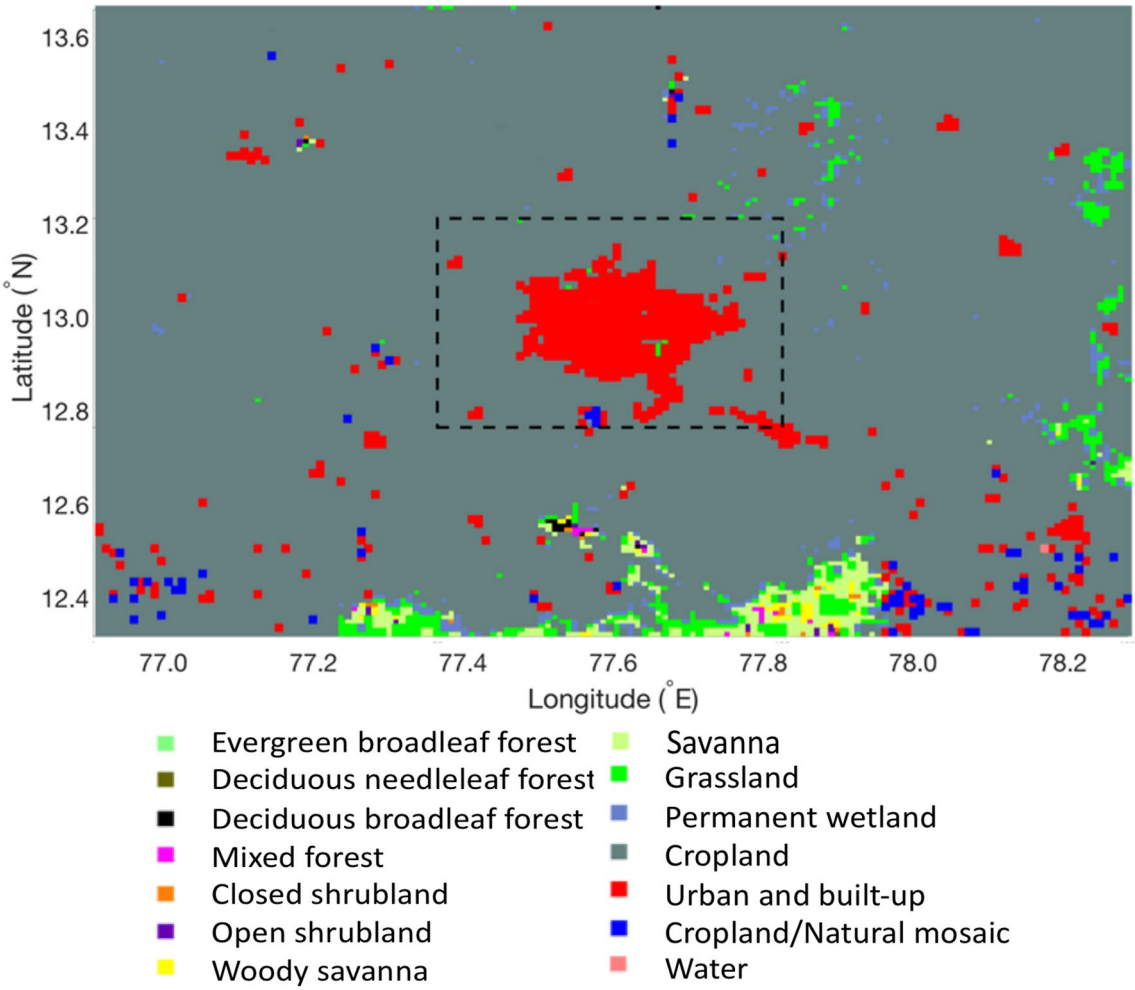

Fig. 2 The 150 km × 150 km domain with 1 km grid spacing used for all WRF simulations. The background shows the 2018 mean MODIS land cover type on the 1 km WRF domain. The black dashed square represents the 50 km × 50 km area used for all analysis

built-up land as grids that have at least 30% of its surface area being impervious (Belward et al. 1999). To be consistent with Sussman et al. 2019, non-urban area was considered to be cropland since it is the dominant land cover type in the surroundings of Bengaluru (Fig. 2). The IGBP defines grids as cropland if at least 60% of the area is cultivated cropland (Belward et al. 1999).

All simulations were forced by hourly, 0.25° ERA5 reanalysis data (Hersbach et al. 2020) and ran with a 6 s timestep. To ensure the WRF-simulated fields follow the large-scale variations in the forcing data in the free troposphere, spectral nudging was used (Liu et al. 2017). Each simulation had 42 vertical levels with the top at 50 hPa and 11 levels below 2 km to better resolve the PBL. The physical parameterizations used for all simulations included Dudhia shortwave radiation (Dudhia 1989), the rapid radiative transfer model (RRTM) for longwave radiation (Mlawer et al. 1997), Thompson microphysics (Thompson et al. 2008), the Eta similarity scheme for the surface layer (Janjić 1994), and the Noah Land Surface model (Chen and Dudhia 2001). No cumulus parameterization was used due to the convective-permitting grid spacing (Liu et al. 2017). The prescribed default values of aerosol concentrations for WRF were used in all simulations.

MODIS LST data

To evaluate WRF performance, the TSK output from each simulation was compared to MODIS land surface (skin) temperature (LST) data as done in Sohrabinia et al. (2012); Xia et al. (2017); Kedia et al. (2021), and others. MODIS LST is the radiometric temperature derived from surface emission, i.e., with emissivity correction, and is closely related to land surface radiative properties (Zhou et al. 2012). Therefore, TSK from WRF is comparable to MODIS LST and any differences can be attributed to differences in the method used for estimation, i.e., MODIS LST measurements are based on optical remote sensing instruments and WRF TSK

estimates are based on numerical calculations and assumptions (Kedia et al. 2021). MODIS LST was chosen in order to be consistent with Sussman et al. (2019) that characterized the UHI over Bengaluru using MODIS. Daily LST data was obtained from Collection 6 of the MODIS instruments Terra (MOD11A1) and Aqua (MYD11A1) at 1 km resolution for the DJF and ASO time periods (Wan 2013). The Sun synchronous orbital characteristics of Terra and Aqua have a daytime equatorial crossing time of approximately 10:30 and 13:30 local solar time and a nighttime equatorial crossing time of approximately 22:30 and 01:30 local solar time. To be consistent with Sussman et al. (2019, 2021), the LST data from Terra and Aqua were averaged to create daytime and nighttime means. In order to compare the WRF simulations to approximately the same diurnal timing as the MODIS observations, the TSK output from WRF was averaged for daytime using the 05:00 and 08:00 UTC output (i.e., 10:30 and 13:30 Indian Standard Time or IST) and for nighttime using the 17:00 and 20:00 UTC output (22:30 and 01:30 IST). All evaluation analyses were carried out over the central 50 km × 50 km region of the WRF domain (Fig. 2), which is the same area analyzed in Sussman et al. (2019, 2021).

MODIS daily data can suffer from gaps in coverage due to its temporal sampling of imaging the entire Earth every 1–2 days. Additionally, MODIS LST data can be missing in cloudy conditions, which can occur often during the wet season in Bengaluru. Therefore, it is necessary to confirm that dates with MODIS data available are also cloud-free in the WRF simulations since the best estimates of LST by MODIS are retrieved under clear-sky conditions (Xia et al. 2017). For each date with MODIS data available, the cloudiness of the WRF simulations was determined. The WRF output of cloud fraction was averaged for 10:30 and 13:30 IST for daytime and 22:30 and 01:30 IST for nighttime for each simulation at each vertical level. If the cloud fraction for any vertical level exceeded 0.05 for 15% or more of the 50 km × 50 km region, that date was classified as cloudy (Ackerman et al. 2008). The number of clear-sky days in WRF that were used in the evaluation are shown in Table 1. As expected, DJF has more dates that can be used compared to ASO since DJF is characterized by mostly dry conditions. Despite the lower number of samples in ASO, more cases can still be evaluated compared to Paul et al. (2018). These results were consistent for all simulations regardless of which UCM or PBL scheme was used.

Table 1 The number of days used for all evaluation analyses for each season and time of day based on the common clear-sky MODIS and WRF dates

	DJF Daytime	ASO Daytime	DJF Nighttime	ASO Nighttime
Number of Days	43	13	37	12

Analysis

The LST bias was computed as the WRF minus MODIS LST difference for each grid in the 50 km × 50 km area for the clear-sky days in each simulation. The temporal correlation coefficient between LST from each simulation and MODIS was also computed at each grid. Significance of the correlation was evaluated using the two-tailed Student's t-test with a p-value ≤ 0.10 to be considered significant. The mean urban LST, non-urban LST, and UHI intensity biases were computed for each simulation. The urban component was computed similarly to Sussman et al. (2019) by matching the urban land cover grids to the LST data, which were both of 1 km resolution, and classifying that as urban LST. The same was done for non-urban LST, but using the cropland grids. Here, these calculations were slightly modified to have the urban and non-urban LST be in their "purest" form. If an urban grid was 2 km or less away from a cropland, grassland, or water grid, it was excluded from the urban LST calculation in an effort to reduce possible contamination of cooler LST from vegetated and water areas. Similarly, if a non-urban grid was 2 km or less away from an urban, grassland, or water grid, it was excluded from the non-urban LST calculation. Similar to Sussman et al. (2019) and other previous studies, the surface UHI intensity was calculated as the mean urban LST minus the mean non-urban LST.

To investigate potential reasons for the LST biases, temporal correlations between WRF LST and WRF surface absorbed shortwave (SW) radiation, surface net longwave (LW) radiation (i.e., downward minus upward LW radiation), and the surface sensible (SH) and latent (LH) heat fluxes over the clear-sky days were computed at each grid. No correlations were computed for absorbed SW radiation and the LH flux at nighttime since the mean values are zero. These variables were chosen since they have a high likelihood of influencing LST as they comprise the surface energy budget (Zhou et al. 2012) and are computed differently in WRF depending on UCM choice; therefore, their differences may be responsible for the LST biases. When using No-UCM, the radiative, LH and SH fluxes over all land cover types are calculated by the Noah Land Surface model (Chen et al. 2011). When WRF is coupled to an UCM, these variables are still calculated by the Noah Land Surface model over non-urban grids, but by the UCM over urban grids. When using an UCM, the urban fraction parameter exists, which represents the sub-grid fraction of an urban grid that is impervious (Chen et al. 2011). Default urban fraction values are 0.95, 0.90, and 0.50 for industrial/commercial, high-intensity residential, and low-intensity residential development. Since urban fraction does not exist in No-UCM, the

urban grids are seen by WRF as 100% impervious urban land cover with no natural vegetation. For the SLUCM and MLUCM simulations, an urban fraction of 0.90 was used for all urban grids, which was chosen since Bengaluru has urban greenness values ranging between 0.05 and 0.25 for DJF and ASO according to the MODIS enhanced vegetation index dataset (Sussman et al. 2019). Therefore, Bengaluru's surface is not completely urban and does have a small amount of natural vegetation. Due to these model differences, the LH flux should be lower for the No-UCM cases compared to the SLUCM and MLUCM cases. Additionally, as mentioned in Sect. "Urbanization modeling", the SLUCM and MLUCM can shadow, trap, and reflect shortwave and longwave radiation in the urban canopy. None of these processes occur when using No-UCM. Therefore, differences in surface radiation may exist due to these different parameterizations.

Results

WRF simulation biases

The mean MODIS LST and WRF biases during DJF daytime are shown in Fig. 3. Consistent with Sussman et al. (2019), the MODIS data has a weak UHI. Sussman et al. (2021) determined that the increased concentration of aerosols over Bengaluru was high enough to make the UHI nearly neutral during DJF daytime by their ability to absorb solar radiation and limit surface warming. Figure 3 shows that the SLUCM has the least urban LST bias of ± 2 °C when used with either PBL scheme. The No-UCM and MLUCM simulations both overestimate urban LST by 1–7 °C with either PBL scheme, with the overestimation about 1 °C for urban areas that had a high LST in the MODIS data. The non-urban LST bias appears consistent across all simulations with most of the area exhibiting an underestimation of 1–3 °C except for the southern portion of the region where some overestimation occurs. For each simulation, all significant temporal correlations with MODIS LST are positive. Correlations > 0.4 typically are located in areas with low mean bias, thus these are areas with high WRF skill.

Figure 4 shows the MODIS mean LST and WRF biases for ASO daytime. Similar to DJF daytime, the SLUCM has the least urban LST bias, regardless of PBL scheme, and the non-urban LST biases are similar across all simulations. Additionally, the high urban LST in MODIS is simulated well by the SLUCM with a bias below 1 °C. In contrast to DJF daytime, WRF overestimates LST over nearly the entire region in ASO daytime. WRF overestimates urban LST by 1–5 °C using the SLUCM and up to 10 °C using No-UCM or the MLUCM, regardless of PBL scheme. Furthermore, the temporal correlations with MODIS are smaller in magnitude and negative compared to DJF daytime, indicating that WRF shows less skill in ASO daytime. The No-UCM simulations have fewer significant temporal correlations compared to the SLUCM and MLUCM.

The MODIS mean LST and WRF biases for DJF nighttime are shown in Fig. 5. Regardless of PBL scheme, the SLUCM has the least urban bias of ± 2 °C and No-UCM has urban biases of 1–6 °C, which is similar to DJF daytime. The MLUCM shows negative urban bias, which is more negative when used with MYJ compared to BouLac. The LST bias over the non-urban areas are mainly negative and of smaller magnitude compared to DJF daytime. Positive temporal correlations exist in all cases and are highest over areas with small mean bias.

The results for ASO nighttime are shown in Fig. 6. Similar to ASO daytime, the urban LST bias is positive for No-UCM and the SLUCM, but slightly negative for the MLUCM. Similar to DJF nighttime, the MLUCM urban LST bias is more negative when used with MYJ. The smallest urban biases occur for the MLUCM of ± 2 °C. Therefore, the MLUCM shows the least urban LST bias in ASO nighttime, whereas in DJF daytime and nighttime and ASO daytime, the SLUCM exhibited the least urban bias. The non-urban LST biases, which are similar across the simulations, are smaller than in ASO daytime, but are still mostly positive. Additionally, some of the significant temporal correlations are positive, which is different from ASO daytime.

Table 2 shows the mean urban LST, non-urban LST, and UHI intensity bias for all simulations based on the land covers in their "purest" form. For non-urban LST, the bias is only PBL dependent and the differences are marginal. Across all simulations, WRF underestimates non-urban LST by approximately 1 °C in DJF daytime and nighttime. This underestimation is slightly larger for MYJ than BouLac. In contrast, WRF overestimates non-urban LST in ASO daytime by ~ 4 °C and nighttime by ~ 1 °C. The overestimation is larger for BouLac than MYJ. In general, for both DJF and ASO, the magnitude of the non-urban LST bias is larger during daytime than nighttime. Unlike 2-m air temperature, LST has higher sensitivity to radiation (Kwok and Ng 2021). Therefore, daytime LST may have increased variability compared to nighttime due to the combined influences of solar and terrestrial radiation and latent and sensible heat fluxes (Dai et al. 1999).

For urban LST, the mean bias varies more with UCM choice than PBL scheme (Table 2). For DJF daytime, the SLUCM has the smallest mean bias with BouLac (− 0.73 °C), which is slightly larger with MYJ (− 0.99 °C). Using No-UCM or the MLUCM produced approximately the same bias with MYJ (2.13 °C and 2.03 °C). In contrast, when BouLac was used, using No-UCM produced smaller bias than the MLUCM (2.43 °C versus 2.74 °C). Similar to DJF daytime, the SLUCM has the smallest mean bias

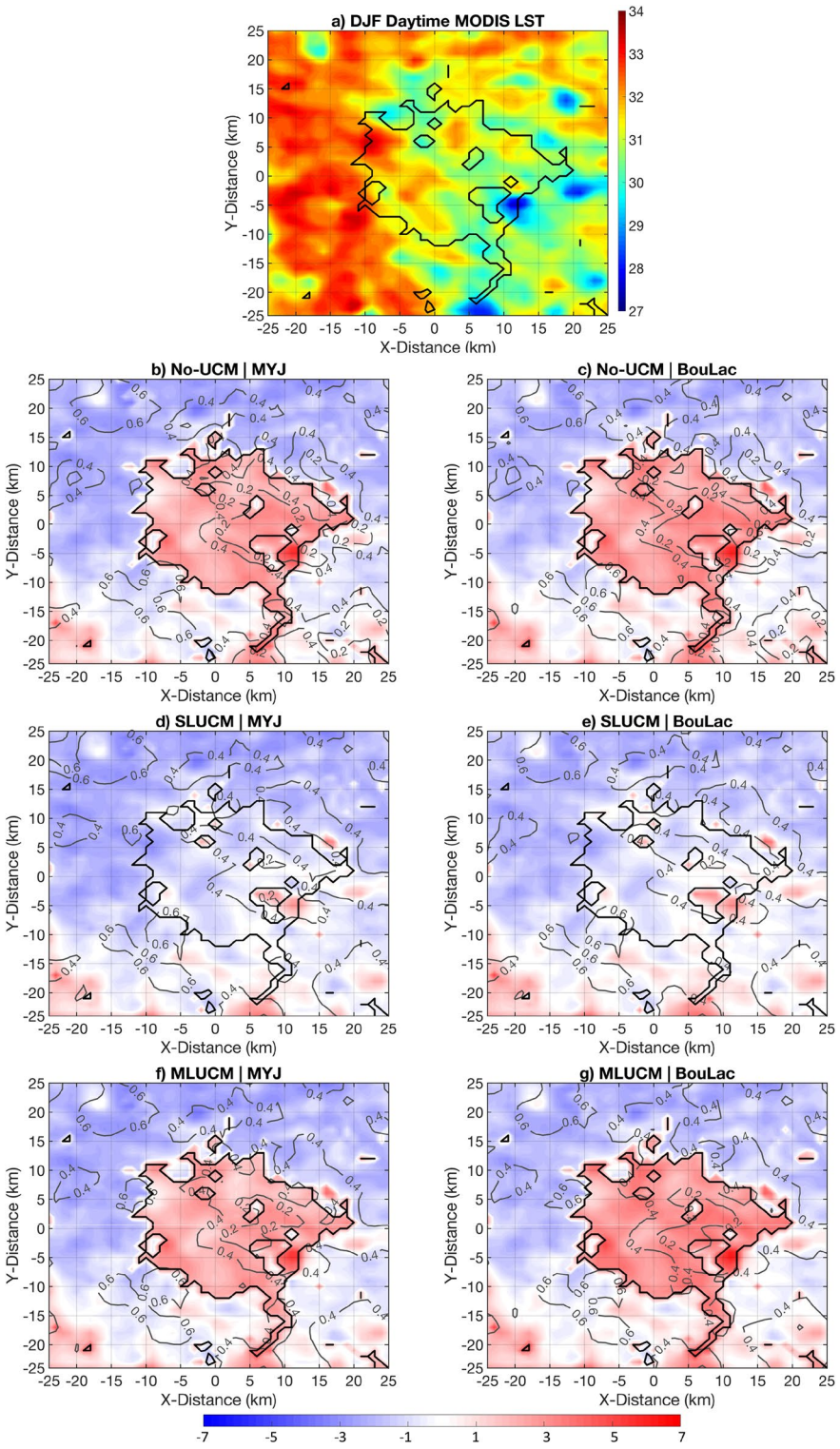

Fig. 3 **a** The daytime mean land surface temperature (LST, in °C) averaged over clear-sky days from 17 December 2017–14 February 2018 (DJF) from the MODIS data for the 50 km × 50 km region surrounding the Bengaluru city center. The black contour outlines the urban boundaries. **b** LST biases relative to MODIS LST (shading, in °C) for DJF daytime using No-UCM with MYJ. Gray contours indicate the value of the temporal correlation at each grid point between the simulation LST and MODIS LST and are plotted only when significant at the 10% level. **c** Same as **b**, but for No-UCM with BouLac. **d–e** Same as **b–c**, but for the SLUCM. **f–g** Same as **b–c**, but for the MLUCM

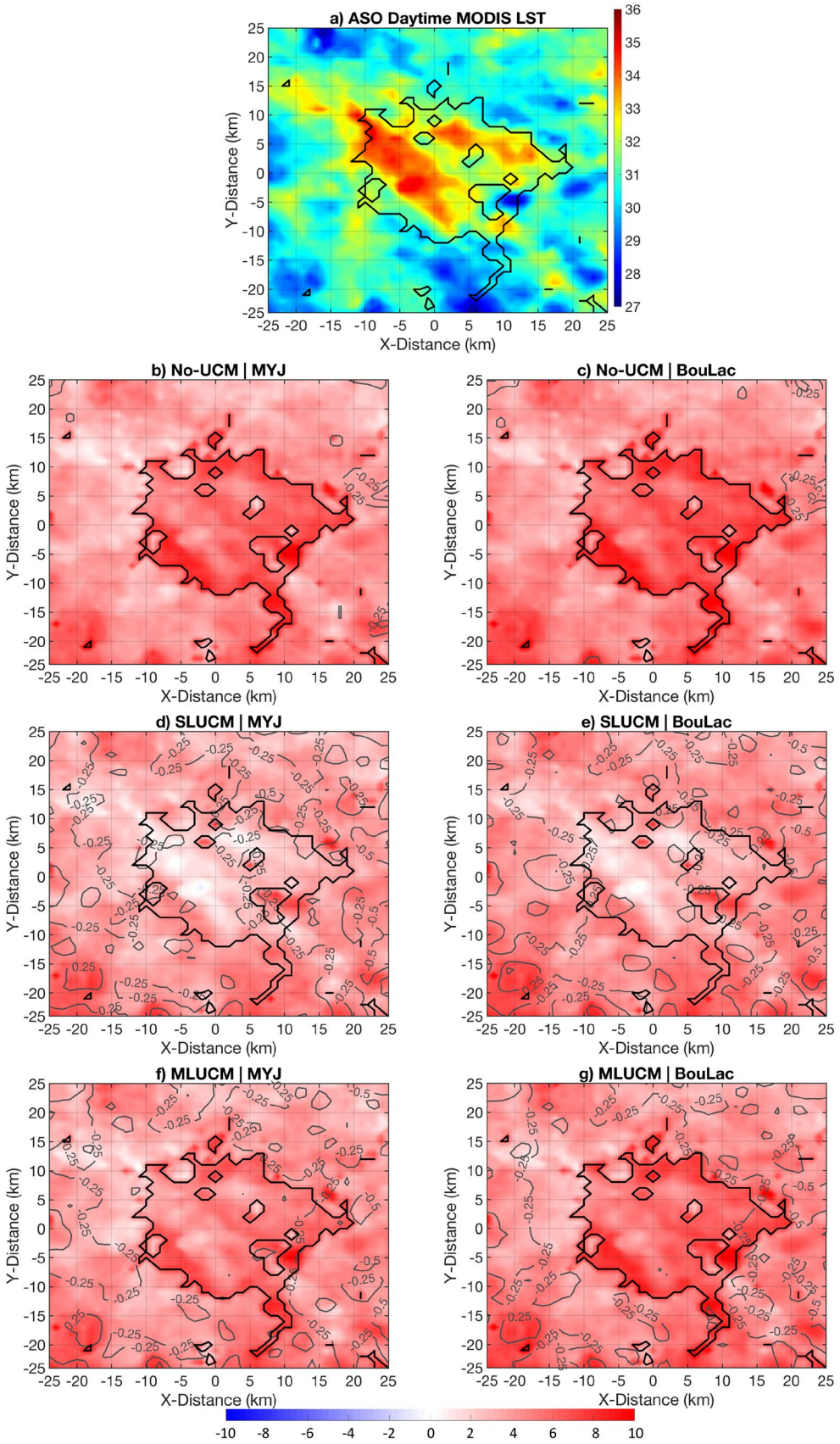

Fig. 4 Same as Fig. 3, but for ASO daytime (i.e., 17 August 2018–15 October 2018)

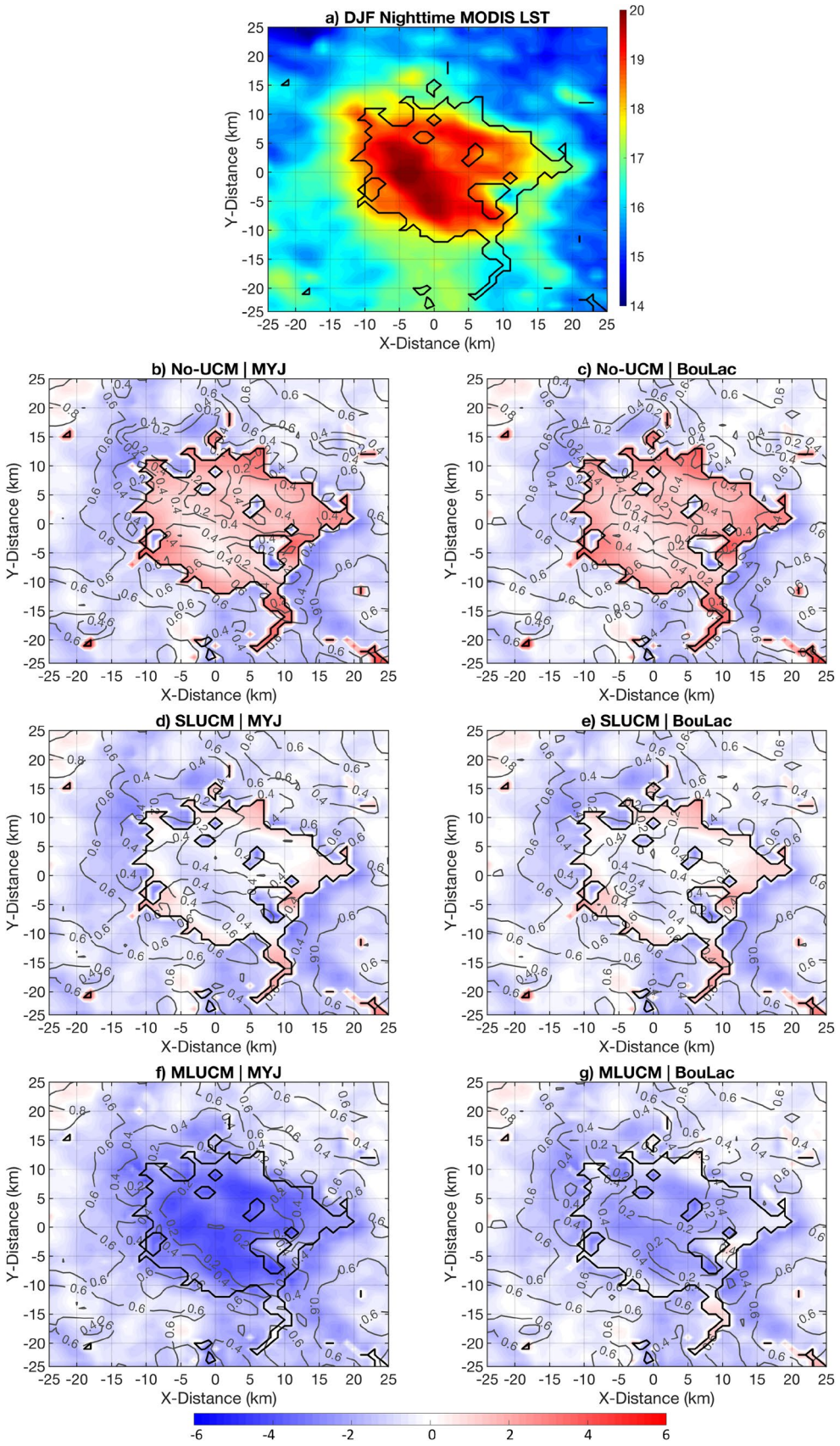

Fig. 5 Same as Fig. 3, but for DJF nighttime

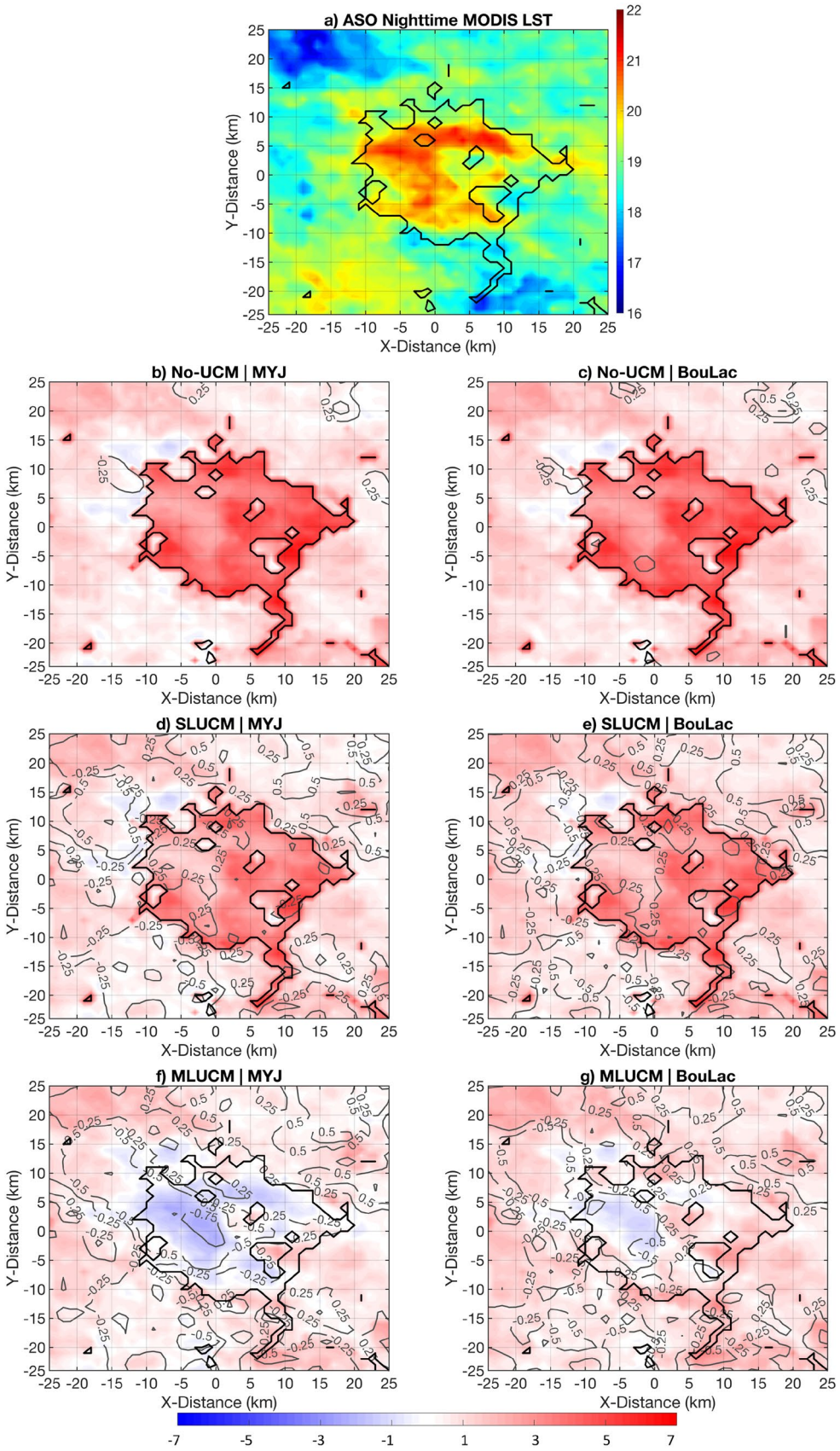

Fig. 6 Same as Fig. 3, but for ASO nighttime

Table 2 Summary of the mean urban LST, non-urban LST, and UHI intensity biases (in °C) for the 12 WRF simulations. Bold indicates the lowest magnitude bias for urban LST, non-urban LST, and UHI intensity during each season and time of day

UCM Option	PBL Scheme	DJF						ASO					
		Day			Night			Day			Night		
		Urban	Non-urban	UHI Intensity	Urban	Non-urban	UHI Intensity	Urban	Non-urban	UHI Intensity	Urban	Non-urban	UHI Intensity
No-UCM	MYJ	2.13	–1.30	3.43	1.21	–0.89	2.10	5.46	3.73	1.73	3.67	0.80	2.87
	BouLac	2.43	–0.99	3.42	1.35	**–0.73**	2.08	6.07	4.27	1.80	3.74	1.59	2.15
SLUCM	MYJ	–0.99	–1.31	0.32	–0.44	–0.91	**0.47**	**1.88**	**3.66**	–1.78	2.61	0.78	1.83
	BouLac	**–0.73**	–1.01	**0.28**	**–0.27**	–0.74	**0.47**	2.29	4.23	–1.94	2.72	1.57	**1.15**
MLUCM	MYJ	2.03	–1.24	3.27	–3.64	–0.94	–2.70	4.43	3.77	**0.66**	–0.93	**0.74**	–1.67
	BouLac	2.74	**–0.97**	3.71	–2.01	–0.80	–1.21	5.44	4.23	1.21	**0.08**	1.56	–1.48

with BouLac (− 0.27 °C), which is slightly larger with MYJ (− 0.44 °C) in DJF nighttime. In contrast to DJF daytime, the mean urban LST bias is negative in DJF nighttime with the MLUCM for both MYJ (− 3.64 °C) and BouLac (− 2.01 °C). Similar mean biases result when using No-UCM with MYJ (1.21 °C) or BouLac (1.35 °C) for DJF nighttime. For ASO daytime, the SLUCM has the smallest urban LST bias with MYJ (1.88 °C), which is slightly larger with BouLac (2.29 °C). The large positive bias for the MLUCM was slightly less with MYJ (4.43 °C) than with BouLac (5.44 °C). Similarly, the positive bias for No-UCM was smaller with MYJ (5.46 °C) than with BouLac (6.07 °C) in ASO daytime. For ASO nighttime, the MLUCM has the smallest mean bias with BouLac (0.08 °C), which becomes slightly negative (− 0.93 °C) with MYJ. The bias produced with the SLUCM was positive and about the same for MYJ (2.61 °C) and BouLac (2.72 °C). Similarly, the bias produced with No-UCM was about the same for MYJ (3.67 °C) and BouLac (3.74 °C). Similar to the non-urban LST biases, the urban LST bias is generally larger in daytime than at nighttime.

Since the biases in non-urban LST are approximately the same and insensitive to UCM and PBL scheme, it is expected that the same physics combination that produced the smallest bias for urban LST would also produce the smallest bias for UHI intensity. This is true for DJF daytime and nighttime, but not for ASO daytime and nighttime (Table 2). For ASO daytime, the smallest UHI intensity bias of 0.66 °C occurred for the MLUCM with MYJ, rather than the SLUCM with MYJ that produced the smallest urban LST bias. This discrepancy results from the urban and non-urban biases being similar to each other when using the MLUCM with MYJ, even though the individual biases are higher for both urban and non-urban LST when using the SLUCM with MYJ. For ASO nighttime, the lowest bias for UHI intensity of 1.15 °C occurred for the SLUCM with BouLac, rather than the MLUCM with BouLac that had the smallest urban LST bias. Again, this discrepancy results from the urban and non-urban biases being similar to each other when using the SLUCM with BouLac, even though the urban and non-urban biases are both larger than the MLUCM with BouLac case. Thus, the UHI intensity bias depends on the bias difference between the urban and non-urban biases, rather than the urban LST bias alone.

Potential contributing factors to LST biases

Figures 7, 8, 9, 10 show the mean simulated LST, surface absorbed SW radiation, net surface LW radiation, and the surface SH and LH fluxes for each UCM with BouLac for each season and time of day. Also shown are the grids that have a significant temporal correlation coefficient between the variable shown and LST of magnitude 0.50 or greater,

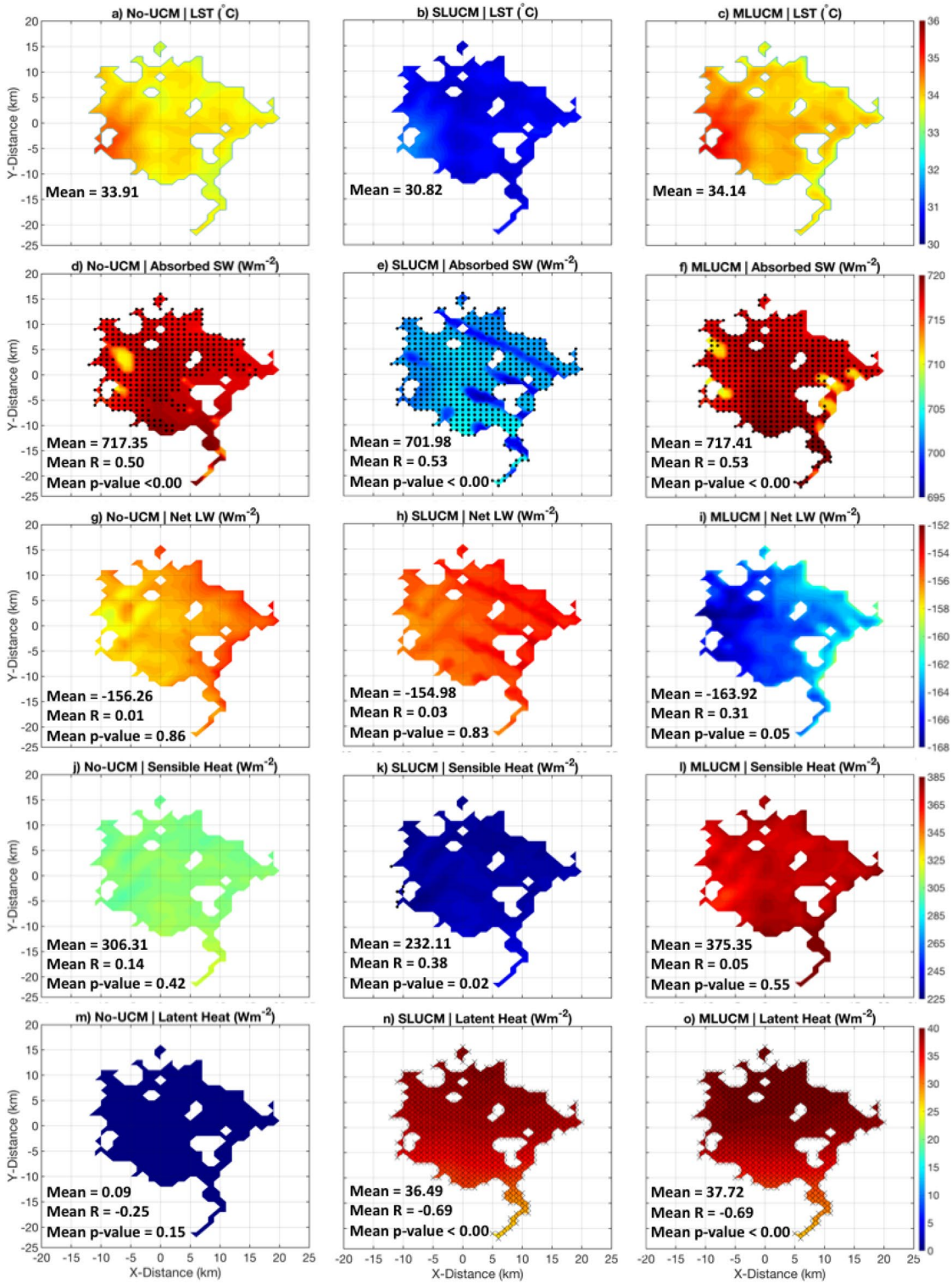

Fig. 7 **a**–**c** The mean daytime land surface temperature (LST, in °C) averaged over clear-sky days from 17 December 2017–14 February 2018 (DJF) using **a** No-UCM, **b** the SLUCM, and **c** the MLUCM with BouLac over Bengaluru. **d**–**f** Same as **a**–**c**, but for DJF daytime absorbed shortwave (SW) radiation at the surface (positive downward, in Wm^{-2}). **g**–**i** Same as **a**–**c**, but for DJF daytime net surface longwave (LW) radiation (negative upward, Wm^{-2}). **j**–**l** Same as **a**–**c**, but for DJF daytime surface sensible heat flux (positive upward, in Wm^{-2}. (m–o) Same as **a**–**c**, but for DJF daytime surface latent heat flux (positive upward, in Wm^{-2}). Stippling indicates that the temporal correlation between LST and the variable shown is > 0.50 and significant at the 10% level. A cross indicates that the temporal correlation between LST and the variable shown is < –0.50 and significant at the 10% level. The mean value for each variable, mean correlation (R) with LST, and associated mean p-value averaged over the city are shown in each panel

thus indicating a strong relationship. This analysis was done only over the main area of Bengaluru since Figs. 3, 4, 5, 6 showed non-urban LST to be insensitive to physics choice, which is attributable to the Noah Land Surface model calculating the radiative and surface fluxes in each case. The mean values of each variable over the city and the mean correlation with LST and associated p-value are shown. Only the results for the BouLac PBL scheme are presented since the simulated LST over Bengaluru has little sensitivity to PBL scheme and three of the four season and time of day cases showed BouLac to perform best (Table 2).

For DJF daytime (Fig. 7), the mean LST is highest for the MLUCM (34.14 °C), followed by No-UCM (33.91 °C) and the SLUCM (30.82 °C), which matches the urban LST biases (Table 2). These LST differences are consistent with absorbed SW radiation (Fig. 7d–f), which is highest for the MLUCM (717.41 Wm^{-2}), slightly less for No-UCM (717.35 Wm^{-2}), and smallest for the SLUCM (701.98 Wm^{-2}). The DJF daytime LST is strongly correlated with absorbed SW radiation in each case over most of Bengaluru with a mean correlation of 0.53 in the SLUCM and MLUCM and 0.50 for No-UCM. These results suggest that the DJF daytime LST bias is likely partly caused by the amount of absorbed SW radiation. Since the SLUCM and MLUCM can both trap SW radiation, it seems that the MLUCM traps more, given that the surface albedo is similar for both UCMs (mean albedo of 0.167 in SLUCM and 0.165 in MLUCM). Thus, a higher absorbed SW radiation and LST occur in the MLUCM compared to the SLUCM. No-UCM has a high absorbed SW radiation since the urban surfaces are seen as entirely impervious, which allows for more absorption since the urban surface has a lower albedo of 0.15 compared to the SLUCM and MLUCM. Net LW radiation illustrates whether the ground is cooling or warming by thermal radiation. For net LW radiation in DJF daytime (Fig. 7g–i), all UCMs have a negative mean value. Even though there is ground cooling through thermal emission, the mean net radiation (i.e., absorbed SW plus net LW) values are positive for each UCM, which is expected during daytime. The negative net LW radiation values indicate there is less downward LW radiation than upward, which is typical of cloud-free conditions, and therefore, the net LW radiation value is mainly indicative of the upward LW flux. The mean magnitudes are consistent with LST, i.e., the highest is for the MLUCM (–163.92 Wm^{-2}), followed by No-UCM (–156.26 Wm^{-2}) and SLUCM (–154.98 Wm^{-2}), which is a consequence of the Stefan-Boltzmann Law. Additionally, since the SLUCM and MLUCM can both trap LW radiation, it is possible that the MLUCM traps more, which leads to a higher LST and more upward LW radiation to be emitted in MLUCM. However, for all UCMs, none of the grids meet the criteria; therefore, net LW radiation is unlikely a driver of the LST bias. The surface SH flux mainly depends on the gradient between LST and near-surface air temperature. During daytime when solar heating dominates, the ground warms more than the lower atmosphere which causes an upward (i.e., positive) SH flux and high LST. Figure 7j–l shows a positive SH flux for all UCMs since there is no temperature inversion for any of the UCMs (not shown). The mean magnitudes are consistent with LST, i.e., the MLUCM is highest (375.35 Wm^{-2}), followed by No-UCM (306.31 Wm^{-2}) and SLUCM (232.11 Wm^{-2}). However, the SH flux has no grids meeting the criteria; therefore, the SH flux is unlikely a driver of the LST bias in DJF daytime. The LH flux is influenced by vegetation density, the amount of evapotranspiration, and absorbed SW radiation. The MLUCM shows the largest LH mean of 37.72 Wm^{-2} since it has the highest absorbed SW radiation and each urban grid has 10% of its area as pervious (Fig. 7o). The SLUCM has a slightly lower LH mean of 36.49 Wm^{-2} (Fig. 7n). Despite the lower SW radiation in the SLUCM compared to the MLUCM, the SLUCM also has the urban fraction parameter, thus causing a slightly lower LH flux. For No-UCM (Fig. 7m), the LH flux mean is near-zero (0.09 Wm^{-2}), which is a consequence of having no pervious material over the urban grids. All of Bengaluru's grids meet the criteria in the SLUCM and MLUCM. Despite no grids meeting the criteria in No-UCM, which is mainly due to little temporal variation in it's the LH flux, the low LH indicates limited evaporative cooling of the surface, which contributes to the high LST bias.

Figure 8 shows that in ASO daytime, the mean LST is highest for No-UCM (39.30 °C), followed by the MLUCM (38.63 °C) and SLUCM (35.60 °C), which matches the urban LST biases (Table 2). The absorbed SW radiation (Fig. 8d–f) does not show a systematic pattern difference among the cases, but the mean values match with LST with the highest for No-UCM (778.70 Wm^{-2}), followed by MLUCM (771.80 Wm^{-2}) and SLUCM (769.15 Wm^{-2}). Less urban grids meet the criteria for absorbed SW radiation compared to DJF daytime. Therefore, absorbed SW radiation likely plays a smaller role in driving the LST bias in ASO daytime compared to DJF daytime. For net LW radiation (Fig. 8g–i), the mean values are similar for No-UCM (–141.17 Wm^{-2}) and the MLUCM (–141.99 Wm^{-2}), and are slightly lower for the SLUCM (–134.16 Wm^{-2}). Therefore, No-UCM and the MLUCM have more longwave cooling than the SLUCM. Since No-UCM and the MLUCM have a higher LST than the SLUCM, the upward LW flux is higher for those cases (not shown). As with DJF daytime, it is possible the MLUCM is trapping more LW radiation than the SLUCM, leading to a higher LST. The MLUCM has grids meeting the criteria throughout most of Bengaluru, and numerous grids meet the criteria in No-UCM and SLUCM. Therefore, net LW radiation likely plays a role in determining the LST bias in ASO daytime. For the SH flux (Fig. 8j–l), the mean value

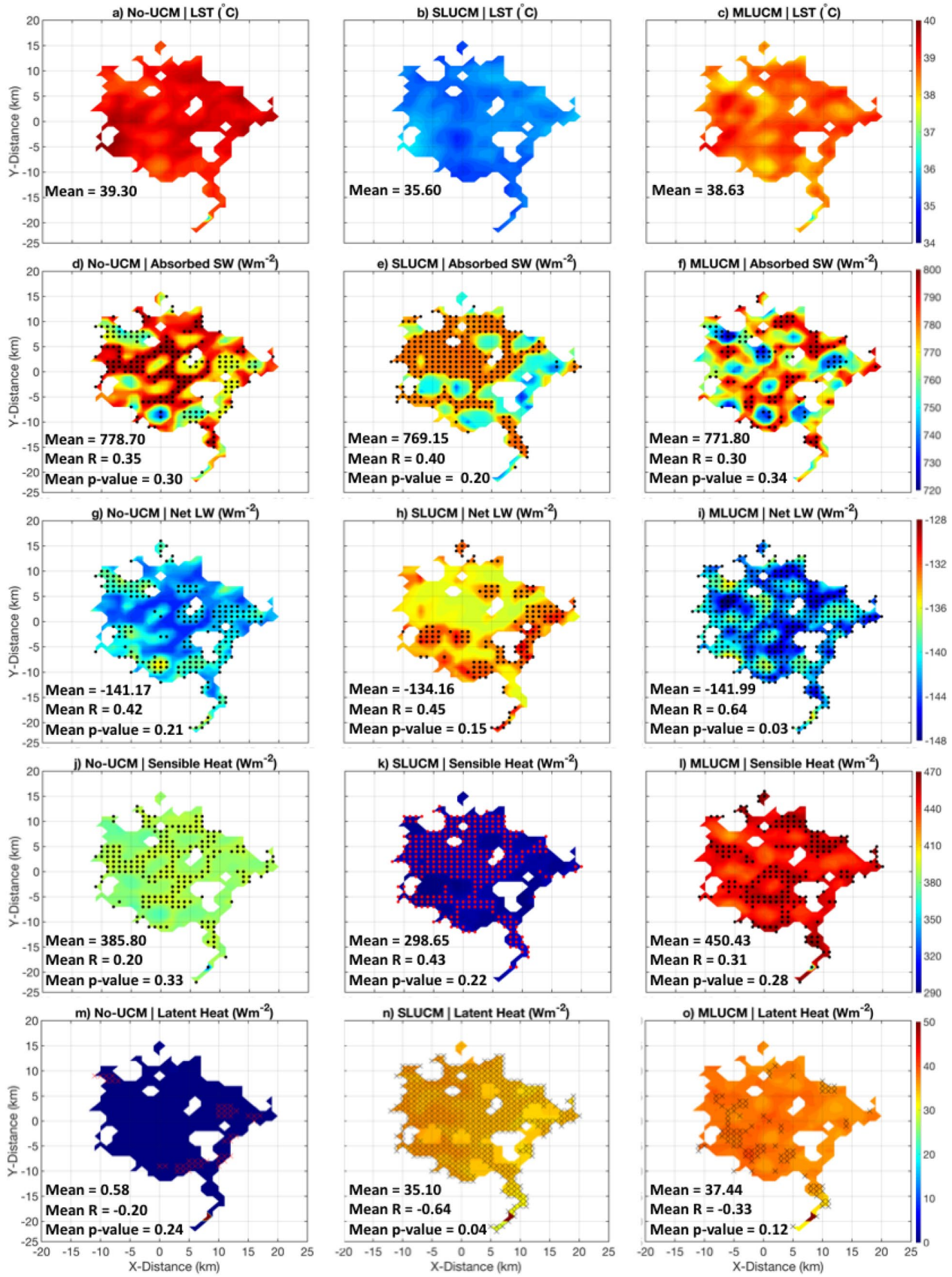

Fig. 8 Same as Fig. 7, but for ASO daytime (i.e., 17 August 2018–15 October 2018). Stippling and crosses are in red for (k) and (m) for visualization purposes only

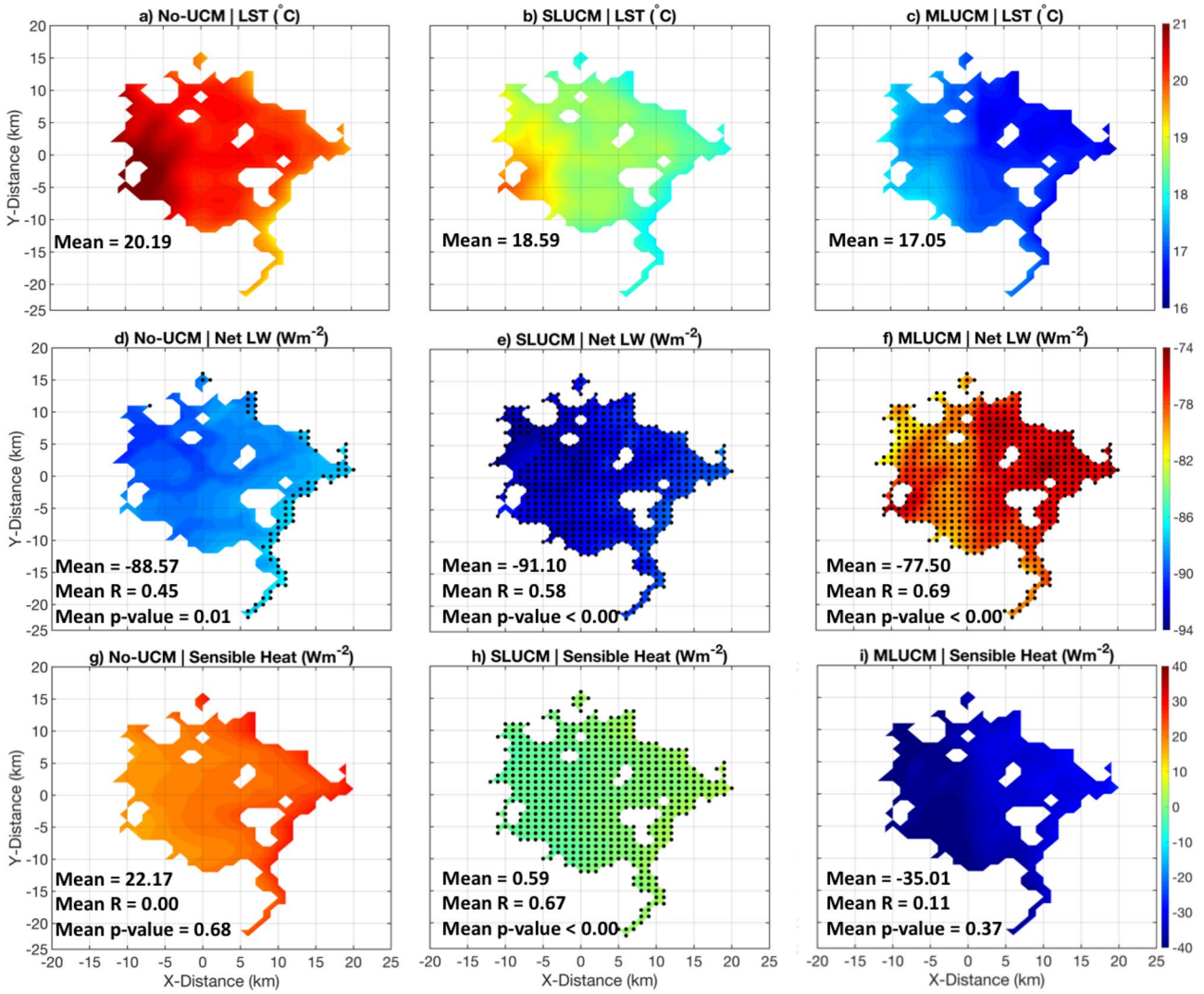

Fig. 9 **a**–**c** The mean nighttime land surface temperature (LST, in °C) averaged over clear-sky days from 17 December 2017–14 February 2018 (DJF) using **a** No-UCM, **b** the SLUCM, and **c** the MLUCM with BouLac over Bengaluru. **d**–**f** Same as **a**–**c**, but for DJF nighttime net surface longwave (LW) radiation (negative upward, in Wm^{-2}). **g**–**i** Same as **a**–**c**, but for DJF nighttime surface sensible heat flux (positive upward, in Wm^{-2}). Stippling indicates that the temporal correlation between LST and the variable of interest is > 0.50 and significant at the 10% level. The mean value for each variable, mean correlation (R) with LST, and associated mean p-value averaged over the city are shown in each panel

is highest for the MLUCM (450.43 Wm^{-2}), followed by No-UCM (385.80 Wm^{-2}) and SLUCM (298.65 Wm^{-2}). The high SH mean in the MLUCM is likely a result of LW trapping causing the surface to be much warmer than the near-surface, whereas in SLUCM, the LST and near-surface air temperature are similar (not shown), which allows for a smaller SH flux. Therefore, the SH flux is a consequence of LW radiation influencing LST, rather than the flux being a driver of the bias. For the LH flux (Fig. 8m–o), the results are similar to DJF daytime except that a few grids meet the criteria in No-UCM, less grids meet the criteria in the SLUCM and MLUCM, and the correlation is stronger in the SLUCM (mean R = –0.64) compared to the MLUCM (mean $R = -0.33$), whereas the correlation was the same for the SLUCM and MLUCM in DJF daytime (mean $R = -0.69$). Therefore, the LH flux also plays a role in the LST bias for ASO daytime.

For DJF nighttime (Fig. 9), the mean LST is highest for No-UCM (too warm), followed by the SLUCM, and the MLUCM (too cold). The net LW radiation (Fig. 9d–f) is highest for the SLUCM (–91.10 Wm^{-2}), followed by No-UCM (–88.57 Wm^{-2}) and the MLUCM (–77.50 Wm^{-2}). Most of Bengaluru has grids meeting the criteria for net LW in the SLUCM and MLUCM, but only a few in No-UCM. During DJF daytime, it was found that the MLUCM likely traps more LW radiation than the SLUCM, causing

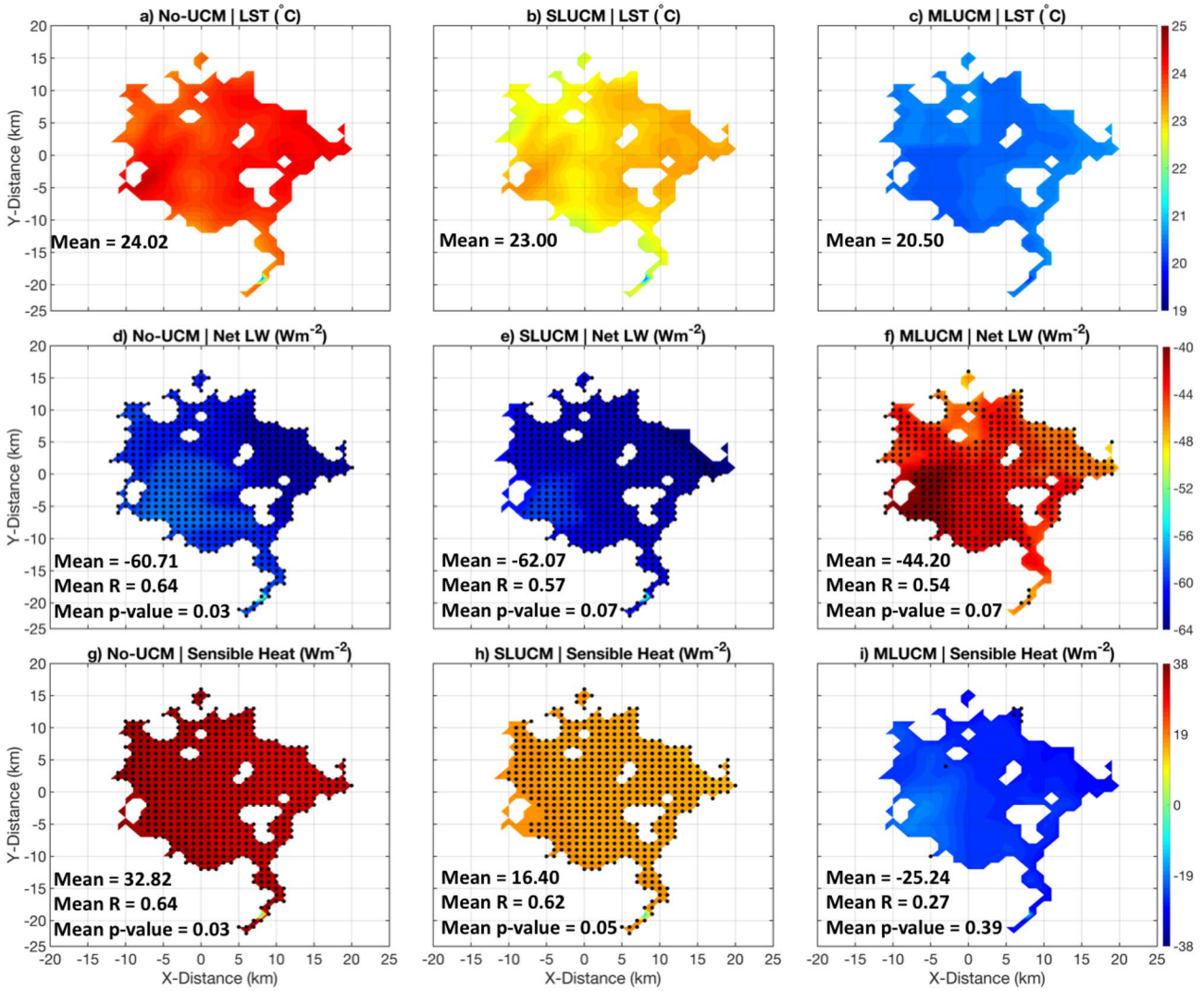

Fig. 10 Same as Fig. 9, but for ASO nighttime (i.e., 17 August 2018–15 October 2018)

a higher LST bias for the MLUCM and a higher magnitude net LW flux (i.e., more upward LW radiation). As a consequence of large LW cooling during DJF daytime, the LST and net LW radiation are lower in MLUCM than in No-UCM and the SLUCM during nighttime. Since the net LW radiation was similar during DJF daytime for No-UCM and the SLUCM, the values continue to be similar during DJF nighttime. Therefore, net LW radiation seems to play a major role in determining the LST bias during DJF nighttime. During nighttime, the SH flux is often weaker than during daytime as heat stored during the day is released, which often warms the lower atmosphere and decreases LST. For SH (Fig. 9g–i), the mean is highest for No-UCM (22.17 Wm^{-2}), followed by the SLUCM (0.59 Wm^{-2}) and MLUCM (–35.01 Wm^{-2}), which matches the ordering of the LST means. The negative SH flux in the MLUCM is indicative of a temperature inversion (not shown). This could be an effect of how the MLUCM handles LW radiation. Since the MLUCM trapped a high amount of LW radiation during DJF daytime, which led to a high magnitude net LW radiation (i.e., upward LW flux), this warmed the lower levels and cooled the surface at nighttime. Only the SLUCM has grids meeting the criteria for SH, in which the criteria is met for the entire city. Similar to daytime, the SH flux value appears to be a consequence of LW radiation rather than a cause of the LST bias.

The mean LST for ASO nighttime (Fig. 10a–c) is highest is for No-UCM (24.02 °C), followed by the SLUCM (23.00 °C) and the MLUCM (20.50 °C), which matches the urban LST biases (Table 2). For net LW radiation (Fig. 10d–f), the results are similar to DJF nighttime with the highest mean for the SLUCM (–62.07 Wm^{-2}), followed by No-UCM (–60.71 Wm^{-2}) and the MLUCM (–44.20 Wm^{-2}). However, more grids meet the criteria in No-UCM compared

to DJF nighttime. Therefore, again it is likely that since the MLUCM traps a high amount of LW radiation during the day causing more thermal emission, the net LW radiative flux and LST are lower compared to the other UCMs at nighttime. However, unlike DJF nighttime, the MLUCM has the lowest urban LST bias in ASO nighttime (Table 2), indicating the processes are most accurate for the MLUCM. For SH (Fig. 10g–i), the results are again similar to DJF nighttime with the highest mean for No-UCM (32.82 Wm^{-2}), followed by the SLUCM (16.40 Wm^{-2}) and MLUCM (–25.24 Wm^{-2}). In contrast to DJF nighttime, the respective mean values are all higher, most of the city in No-UCM and the SLUCM has grids meeting the criteria, and a few grids in the MLUCM meet the criteria now. Again, the negative SH flux in the MLUCM corresponds to a temperature inversion (not shown), which is likely due to high LW radiation emission during the day which warms the lower levels more than the surface. Similar to the other cases, the SH flux seems to be an effect of LW radiation and LST rather than a cause of the LST bias.

The above results suggest that the MLUCM may trap too much SW and LW radiation during daytime, which may contribute to its large positive daytime LST biases. The large trapping of LW radiation by the MLUCM during daytime leads to a high upward LW flux during daytime, which causes a cool nighttime LST, a low net LW flux magnitude at nighttime, and a negative SH flux at nighttime due to a warmer lower atmosphere compared to the surface. These consequences in MLUCM may partially be due to better interaction between the urban canopy and PBL compared to the other UCMs. Additionally, due to no pervious area over the urban surface in No-UCM, the daytime LH flux is near-zero in both DJF and ASO, which contributes to the high daytime LST bias in No-UCM. The SLUCM and MLUCM produce similar LH values since they both have the urban fraction parameter. Overall, the SLUCM has the least urban LST bias during daytime in both seasons due to a higher LH flux compared to No-UCM and less absorbed SW radiation and trapping of LW radiation compared to MLUCM. In DJF nighttime, the SLUCM has the least urban LST bias since the LST in the MLUCM cooled too much due to high thermal emission during the daytime. In ASO nighttime, the MLUCM has the lowest urban LST, indicating that the LW radiation processes are fairly accurate in this case.

Conclusions

In this study, WRF simulations over Bengaluru, India were performed to test the model's ability in simulating LST in comparison with MODIS data. This study evaluated WRF with No-UCM, and the coupling to the SLUCM and MLUCM with the MYJ and BouLac PBL schemes. The differences in model physics were used to help explain the resulting LST biases. The evaluation was done separately for daytime and nighttime during the dry (DJF) and wet (ASO) seasons.

Results show that coupling WRF to an UCM reduced the simulated urban LST bias, which led to improved simulations of the UHI. This is consistent with previous studies (e.g., Bhati and Mohan 2018). For the best case, urban LST was underestimated by less than 1 °C during DJF daytime and nighttime, and was overestimated by 1.88 °C and 0.08 °C in ASO daytime and nighttime, which are suggestive of valid model results due to the low biases (Table 2). Urban LST and UHI intensity were found to not be strongly sensitive to PBL scheme. Non-urban LST was mainly insensitive to both UCM and PBL choice. The two cases that were sensitive to PBL choice occurred when WRF was coupled to the MLUCM during nighttime for both seasons, in which the urban LST bias was more positive with BouLac than MYJ (Table 2). In general, urban LST and UHI intensity were found to be simulated best using the SLUCM. This suggests that the more computationally expensive MLUCM often does not need to be used. Furthermore, the BEP + BEM, which was not evaluated here, likely is not necessary unless sophisticated UHI mitigation strategies are being tested.

Since WRF's performance was mainly influenced by UCM choice, the UCM differences in how radiative and surface fluxes are calculated were used to explain the LST biases. During daytime, No-UCM had a near-zero LH flux since the urban surfaces have no pervious area, which led to a high LST bias for both seasons. Additionally, the MLUCM traps too much SW radiation and the No-UCM absorbs too much SW radiation due to a lower albedo, both leading to higher LST biases compared to the SLUCM. During nighttime, the LST in MLUCM cools due to high LW emission during the day, which warms the lower atmosphere and causes a temperature inversion and lower LST. This process results in a negative LST bias for MLUCM in DJF nighttime (–2.01 °C), but only a small bias for ASO nighttime (0.08 °C), indicating that this process is accurate in ASO.

Future studies can evaluate other WRF modeling sensitivities, such as the inclusion of an urban morphology dataset. These data can classify urban land cover into several categories based on degree of urbanization. Occasionally, cities have been able to accurately map their urban geometry and can provide these data for numerical modeling. However, these data can be hard to obtain and typically are unavailable in developing countries (Kwok and Ng 2021). Some studies have used databases that relied on machine learning techniques to classify urban land cover into multiple categories, such as the National Land Cover Database (NLCD; Homer et al. 2015) for the United States and the Coordination of Information on the Environment (CORINE) Land Cover inventory (Büttner et al. 2004) for Europe. A recent

initiative is the World Urban Database and Access Portal Tools (WUDAPT; Ching et al. 2018) that works to provide a standardized database on urban morphology using an open source procedure. Urban morphology datasets are difficult to obtain for many Indian cities. To our knowledge, only Bhati and Mohan (2018) has incorporated an urban morphology dataset. Bhati and Mohan (2018) evaluated WRF with urban morphology and WRF with land cover datasets from MODIS and the United States Geological Survey (USGS) using homogeneous urban land cover over New Delhi, in which they found improvements in the simulation of near-surface temperature using urban morphology. No urban morphology dataset was used in this study so that it could be understood how well WRF performs when urban land cover is considered to be homogeneous and using default WRF parameters. While WRF exhibited decent skill in simulating LST, using an urban morphology dataset would likely improve results since the urban fraction parameter could be better tuned for each urban grid.

Other sensitivities that could be explored are the use of WRF-Chem and testing of other PBL schemes with the SLUCM. WRF-Chem allows for the simultaneous integration of the emission, transport, mixing, and chemical transformation of trace gases and aerosols with meteorology. Inclusion of the impact of prognostic aerosols may improve the simulations since anthropogenic aerosols could play a role in impacting urban LST. WRF-Chem was not used here since it was found that aerosol optical depth (AOD) has a low importance in determining urban LST for Bengaluru (Sussman et al. 2021). Since the number of PBL schemes that can be used with the MLUCM is limited, but the SLUCM performed best, it may be worthwhile to test the SLUCM with the other available PBL schemes since the PBL is crucial in urban climate (Garratt 1994).

Overall, the simulations shown here present the first UCM evaluation for India in terms of LST using WRF's default options, and thus give a baseline understanding. Future studies should systematically investigate how other WRF options may improve biases compared to these simulations. Thoroughly evaluating each of these sensitivities will help to ensure that studies investigating mechanisms and mitigation strategies of UHIs use the best possible and most efficient WRF setup available.

Author contributions HS conceptualized the study. HS and AR performed the simulations and initial discussion of results. AD and LZ helped refine the methods. HS performed the calculations, made the figures, and wrote the first draft of this manuscript. AD, AR, and LZ helped revise this manuscript and provided feedback.

Funding The research effort of HS is supported by the Science, Mathematics, and Research for Transformation (SMART) fellowship from the Department of Defense. AD acknowledges funding support from the National Science Foundation (grant nos. AGS-1353740 and OISE-1743738). LZ acknowledges funding support from the National Science Foundation (grant nos. AGS-1952745 and AGS-1854486).

Data availability The MODIS Terra and Aqua combined land cover dataset is available from https://e4ftl01.cr.usgs.gov/MOTA/MCD12Q2.006/2018.01.01/. The MODIS LST dataset is available from https://e4ftl01.cr.usgs.gov/MOLT/MOD11A2.061/ for Terra and https://e4ftl01.cr.usgs.gov/MOLA/MYD11A2.061/ for Aqua. The ERA5 reanalysis data is available from https://cds.climate.copernicus.eu/cdsapp#!/dataset/reanalysis-era5-pressure-levels?tab=overview for pressure level data and https://cds.climate.copernicus.eu/cdsapp#!/dataset/reanalysis-era5-single-levels?tab=overview for surface data. The WRF model can be downloaded from https://www.mmm.ucar.edu/models/wrf. The simulations presented in this study can be made available by contacting Heather Sussman (Heather.S.Sussman@usace.army.mil).

Code availability All analyses and figure creations were carried out in MATLAB by MathWorks (https://www.mathworks.com/products/matlab.html). Code used for this study can be made available by contacting Heather Sussman (Heather.S.Sussman@usace.army.mil).

Declarations

Conflict of interest On behalf of all authors, the corresponding author states that there is no conflict of interest.

References

Ackerman SA, Holz RE, Frey R et al (2008) Cloud detection with MODIS. Part II: validation. J Atmos Ocean Technol 25:1073–1086. https://doi.org/10.1175/2007JTECHA1053.1

Ajilesh P, Rakesh V, Sahoo SK, Himesh S (2019) Observed and model-simulated thermodynamic processes associated with urban heavy rainfall events over Bangalore, India. Meteorol Appl 27:e1854. https://doi.org/10.1002/met.1854

Andersson E (2006) Urban landscapes and sustainable cities. Ecol Soc 11:34. https://doi.org/10.5751/ES-01639-110134

Banks RF, Tiana-Alsina J, Rocadenbosch F, Baldasano JM (2015) Performance evaluation of the boundary-layer height from Lidar and the weather research and forecasting model at an urban coastal site in the north-East Iberian Peninsula. Bound-Layer Meteorol 157:265–292. https://doi.org/10.1007/s10546-015-0056-2

Belward AS, Estes JE, Kilne KD (1999) The IGBP-DIS global 1-km land-cover data set DISCover: a project overview. Photogramm Eng Remote Sensing 65:1013–1020

Bhati S, Mohan M (2018) WRF-urban canopy model evaluation for the assessment of heat island and thermal comfort over an urban airshed in India under varying land use/land cover conditions. Geosci Lett 5:27. https://doi.org/10.1186/s40562-018-0126-7

Bougeault P, Lacarrerè P (1989) Parameterization of orography-induced turbulence in a mesobeta-scale model. Mon Weather Rev 117:1872–1890. https://doi.org/10.1175/1520-0493(1989)117%3C1872:POOITI%3E2.0.CO;2

Büttner G, Feranec J, Jaffrin G et al (2004) The CORINE land cover 2000 project. R. Reuter (Ed.), EARSeL eProceedings, Vol. 3, EARSeL, Paris, pp. 331–346

Chen F, Dudhia J (2001) Coupling an advanced land surface-hydrology model with the Penn State–NCAR MM5 modeling system. Part 1: model implementation and sensitivity. Mon Weather Rev 129:569–585. https://doi.org/10.1175/1520-0493(2001)129%3C0569:CAALSH%3E2.0.CO;2

Chen F, Kusaka H, Bornstein R et al (2011) The integrated WRF/urban modelling system: development, evaluation, and applications to urban environmental problems. Int J Climatol 31:273–288. https://doi.org/10.1002/joc.2158

Ching J, Mills G, Bechtel B et al (2018) World Urban Database and Access Portal Tools (WUDAPT), an urban weather, climate and environmental modeling infrastructure for the Anthropocene. Bull Am Meteorol Soc 99:1907–1924. https://doi.org/10.1175/BAMS-D-16-0236.1

Dai A, Trenberth KE, Karl TR (1999) Effects of clouds, soil moisture, precipitation and water vapor on diurnal temperature range. J Clim 12:2451–2473. https://doi.org/10.1175/1520-0442(1999)012%3C2451:EOCSMP%3E2.0.CO;2

Dudhia J (1989) Numerical study of convection observed during the Winter Monsoon Experiment using a mesoscale two-dimensional model. J Atmos Sci 46:3077–3107. https://doi.org/10.1175/1520-0469(1989)046%3c3077:NSOCOD%3e2.0.CO;2

Ferrero E, Alessandrini S, Vandenberghe F (2018) Assessment of planetary-boundary-layer schemes in the weather research and forecasting model within and above an urban canopy layer. Bound-Layer Meteorol 168:289–319. https://doi.org/10.1007/s10546-018-0349-3

Filho WL, Icaza LE, Neht A et al (2018) Coping with the impacts of urban heat islands. A literature based study on understanding urban heat vulnerability and the need for resilience in cities in a global climate change context. J Clean Prod 171:1140–1149. https://doi.org/10.1016/j.jclepro.2017.10.086

Garratt JR (1994) Review: the atmospheric boundary layer. Earth Sci Rev 37:89–134. https://doi.org/10.1016/0012-8252(94)90026-4

Grimm NB, Faeth SH, Golubiewski NE et al (2008) Global change and the ecology of cities. Science 319:756–760. https://doi.org/10.1126/science.1150195

Hersbach H, Bell B, Berrisford P et al (2020) The ERA5 global reanalysis. Q J R Meteorol Soc 146:1999–2049. https://doi.org/10.1002/qj.3803

Homer C, Dewitz J, Yang L et al (2015) Completion of the 2011 National Land Cover Database for the conterminous United States-Representing a decade of land cover change information. Photogramm Eng Remote Sens 81:345–354

Hung T, Uchihama D, Ochi S, Yasuoka Y (2005) Assessment with satellite data of the urban heat island effects in Asian mega cities. Int J Appl Earth Obs 8:34–48. https://doi.org/10.1016/j.jag.2005.05.003

Imran HM, Kala J, Ng AWM, Muthukumaran S (2018) Effectiveness of green and cool roofs in mitigating urban heat island effects during a heatwave event in the city of Melbourne in southeast Australia. J Clean Prod 197:393–405. https://doi.org/10.1016/j.jclepro.2018.06.179

Jandaghian Z, Beradi U (2020) Comparing urban canopy models for microclimate simulations in weather research and forecasting models. Sustain Cities Soc 55:102025. https://doi.org/10.1016/j.scs.2020.102025

Janjić ZI (1994) The step-mountain Eta coordinate model: further developments of the convection, viscous sublayer and turbulence closure schemes. Mon Wea Rev 122:927–945. https://doi.org/10.1175/1520-0493(1994)122%3C0927:TSMECM%3E2.0.CO;2

Janjić ZI (2002) Nonsingular implementation of the Mellor-Yamada level 2.5 scheme in the NCEP Meso model. In: NCEP Office Note, 437, p. 61. https://www.emc.ncep.noaa.gov/officenotes/newernotes/on437.pdf. Accessed 22 Feb 2022

Kedia S, Bhakare SP, Dwivedi AK et al (2021) Estimates of change in surface meteorology and urban heat island over northwest India: impact of urbanization. Urban Clim 36:100782. https://doi.org/10.1016/j.uclim.2021.100782

Kishtawal CM, Niyogi D, Tewari M et al (2010) Urbanization signature in the observed heavy rainfall climatology over India. Int J Climatol 30:1908–1916. https://doi.org/10.1002/joc.2044

Kusaka H, Kimura F (2004) Coupling a single-layer urban canopy model with a simple atmospheric model: impact on urban heat island simulation for an idealized case. J Meteorol Soc Japan 82:67–80. https://doi.org/10.2151/jmsj.82.67

Kusaka H, Kondo Y, Kikegawa Y, Kimura F (2001) A simple single-layer urban canopy model for atmospheric models: comparison with multi-layer and slab models. Bound-Layer Meteorol 101:329–358. https://doi.org/10.1023/A:1019207923078

Kwok YT, Ng EYY (2021) Trends, topics, and lessons learnt from real case studies using mesoscale atmospheric models for urban climate applications in 2000–2019. Urban Clim 36:100785. https://doi.org/10.1016/j.uclim.2021.100785

Lenzhöler S, Van der Wulp NY (2010) Thermal experience and perception of the built environment in Dutch urban squares. J Urban Des 15:375–401. https://doi.org/10.1080/13574809.2010.488030

Liu Y, Chen F, Warner T, Basara J (2006) Verification of a mesoscale data-assimilation and forecasting system for the Oklahoma City area during the Joint Urban 2003 Field Project. J Appl Meteorol Climatol 45:912–929. https://doi.org/10.1175/JAM2383.1

Liu C, Ikeda K, Rasmussen R et al (2017) Continental-scale convection-permitting modeling of the current and future climate of North America. Clim Dyn 49:71–95. https://doi.org/10.1007/s00382-016-3327-9

Martilli A, Clappier A, Rotach MW (2002) An urban surface exchange parameterization for mesoscale models. Bound Layer Meteorol 104:261–304. https://doi.org/10.1023/A:1016099921195

Mlawer EJ, Taubman SJ, Brown PD et al (1997) Radiative transfer for inhomogeneous atmospheres: RRTM, a validated correlated–k model for the longwave. J Geophys Res 102:16663–16682. https://doi.org/10.1029/97JD00237

Mohan M, Sati AP, Bhati S (2020) Urban sprawl during five decadal period over National Capital Region of India: impact on urban heat island and thermal comfort. Urban Clim 33:100647. https://doi.org/10.1016/j.uclim.2020.100647

Morini E, Touchaei AG, Rossi F et al (2018) Evaluation of albedo enhancement to mitigate impacts of urban heat island in Rome (Italy) using WRF meteorological model. Urban Clim 24:551–566. https://doi.org/10.1016/j.uclim.2017.08.001

Oke TR (1982) The energetic basis of the urban heat island. Q J R Meteorol Soc 108:1–24

Parthasarathy B (1984) Interannual and long-term variability of Indian summer monsoon rainfall. Proc Indian Acad Sci (earth Planet Sci) 93:371–385. https://doi.org/10.1007/BF02843255

Patel P, Karmakar S, Ghosh S, Niyogi D (2020) Improved simulation of very heavy rainfall events by incorporating WUDAPT urban land use/land cover in WRF. Urban Clim 32:100616. https://doi.org/10.1016/j.uclim.2020.100616

Paul S, Ghosh S, Mathew M et al (2018) Increased spatial variability and intensification of extreme monsoon rainfall due to urbanization. Sci Rep 8:3918. https://doi.org/10.1038/s41598-018-22322-9

Rakesh V, Mohapatra GN, Bankar A (2021) Historical extreme rainfall over the Bangalore city, India, on 14 and 15 August 2017: skill of sub-kilometer forecasts from WRF model. Meteorol Atmos Phys 133:1057–1074. https://doi.org/10.1007/s00703-021-00794-1

Ramachandran S, Kedia S, Srivastava R (2012) Aerosol optical depth trends over different regions of India. Atmos Environ 49:338–347. https://doi.org/10.1016/j.atmosenv.2011.11.017

Sahoo SK, Himesh S, Gouda KC (2020) Impact of urbanization on heavy rainfall events: a case study over the megacity of Bengaluru, India. Pure Appl Geophys 177:6029–6049. https://doi.org/10.1007/s00024-020-02624-8

Salamanca F, Martilli A (2010) A new building energy model coupled with an urban canopy parameterization for urban climate

simulations—Part II. Validation with one dimension off-line simulations. Theor Appl Climatol 99:345–356. https://doi.org/10.1007/s00704-009-0142-9

Salamanca F, Martilli A, Tewari M, Chen F (2011) A study of the urban boundary layer using different urban parameterizations and high-resolution urban canopy parameters with WRF. J Appl Meteorol Climatol 50:1107–1128. https://doi.org/10.1175/2010JAMC2538.1

Sati AP, Mohan M (2018) The impact of urbanization during half a century on surface meteorology based on WRF model simulations over National Capital Region, India. Theor Appl Climatol 134:309–323. https://doi.org/10.1007/s00704-017-2275-6

Segura R, Badia A, Venture S et al (2021) Sensitivity study of PBL schemes and soil initialization using the WRF-BEP-BEM model over a Mediterranean coastal city. Urban Clim 39:100982. https://doi.org/10.1016/j.uclim.2021.100982

Shastri H, Paul S, Ghosh S, Karmakar S (2015) Impacts of urbanization on Indian summer monsoon rainfall extremes. J Geophys Res Atmos 120:495–516. https://doi.org/10.1002/2014JD022061

Skamarock WC, Klemp JB, Dudhia J et al (2019) A description of the advanced research WRF version 4. In: NCAR Technical Notes, pp. 145. https://opensky.ucar.edu/islandora/object/opensky%3A2898. Accessed 20 Feb 2022

Sohrabinia M, Rack W, Zawar-Reza P (2012) Analysis of MODIS LST compared with WRF model and in situ data over the Waimakariri River Basin, Canterbury, New Zealand. Remote Sens 4:3501–3527. https://doi.org/10.3390/rs4113501

Sudhira HS, Ramachandra TV, Bala Subrahmanya MH (2007) City profile: Bangalore. Cities 24:379–390. https://doi.org/10.1016/j.cities.2007.04.003

Sussman HS, Raghavendra A, Zhou L (2019) Impacts of increased urbanization on surface temperature, vegetation, and aerosols over Bengaluru, India. Remote Sens Appl Soc Environ 16:100261. https://doi.org/10.1016/j.rsase.2019.100261

Sussman HS, Dai A, Roundy PE (2021) The controlling factors of urban heat in Bengaluru, India. Urban Clim 38:100881. https://doi.org/10.1016/j.uclim.2021.100881

Taha H (1997) Urban climates and heat islands: albedo, evapotranspiration, and anthropogenic heat. Energ Buildings 25:99–103. https://doi.org/10.1016/S0378-7788(96)00999-1

Thompson G, Field PR, Rasmussen RM, Hall WD (2008) Explicit forecasts of winter precipitation using an improved bulk microphysics scheme. Part II: implementation of a new snow parameterization. Mon Weather Rev 136:5095–5115. https://doi.org/10.1175/2008MWR2387.1

van den Berg M, Wendel-Vos W, van Poppel M et al (2015) Health benefits of green spaces in the living environment: a systematic review of epidemiological studies. Urban for Urban Green 14:806–816. https://doi.org/10.1016/j.ufug.2015.07.008

Veena K, Parammasivam KM, Venkatesh TN (2020) Urban heat island studies: current status in India and a comparison with the international studies. J Earth Syst Sci 129:85. https://doi.org/10.1007/s12040-020-1351-y

Wan Z (2013) Collection-6 MODIS land surface temperature products users' guide. pp. 33. https://lpdaac.usgs.gov/documents/118/MOD11_User_Guide_V6.pdf. Accessed 22 Feb 2022

Xia G, Cervarich MC, Baidya Roy S et al (2017) Simulating impacts of real-world wind farms on land surface temperature using the WRF model: validation with observations. Mon Weather Rev 145:4813–4836. https://doi.org/10.1175/MWR-D-16-0401.1

Xie B, Fund CH, Chan A, Lau A (2012) Evaluation of nonlocal and local planetary boundary layer schemes in the WRF model. J Geophys Res 117:D12103. https://doi.org/10.1029/2011JD017080

Zhou L, Dickinson RE, Tian Y et al (2004) Evidence for a significant urbanization effect on climate in China. Proc Natl Acad Sci USA 101:9540–9544. https://doi.org/10.1073/pnas.0400357101

Zhou L, Tian Y, Baidya Roy S et al (2012) Impacts of wind farms on land surface temperature. Nat Clim Change 2:539–543. https://doi.org/10.1038/nclimate1505